Opportunistic Frequency Stability Transfer for Extending the Coherence Time of GNSS Receiver Clocks

Kyle D. Wesson, Kenneth M. Pesyna, Jr., Jahshan A. Bhatti, and Todd E. Humphreys
The University of Texas at Austin, Austin, TX

BIOGRAPHIES

Kyle D. Wesson is pursuing a Ph.D. in the Department of Electrical and Computer Engineering at The University of Texas at Austin. He received his B.S. in Electrical and Computer Engineering from Cornell University. His research interests include indoor navigation and networking.

Kenneth M. Pesyna, Jr., is pursuing a Ph.D. in the Department of Electrical and Computer Engineering at The University of Texas at Austin. He received his B.S. in Electrical and Computer Engineering from Purdue University. His research is in cellular and wireless communications.

Jahshan A. Bhatti is pursuing a Ph.D. in the Department of Aerospace Engineering and Engineering Mechanics at The University of Texas at Austin, where he also received his B.S. His research interests are in the development of small satellites, software-defined radio applications, and GNSS technologies.

Todd E. Humphreys is an assistant professor in the Department of Aerospace Engineering and Engineering Mechanics at The University of Texas at Austin. He received a B.S. and M.S. in Electrical and Computer Engineering from Utah State University and a Ph.D. in Aerospace Engineering from Cornell University. His research interests are in estimation and filtering, GNSS technology, GNSS-based study of the ionosphere and neutral atmosphere, and GNSS security and integrity.

ABSTRACT

A framework is presented for exploiting the frequency stability of non-GNSS signals to extend the coherence time of inexpensive GNSS receiver clocks. This is accomplished by leveraging stable ambient radio frequency signals, called "signals of opportunity," to compensate for the frequency instability of the reference oscillators typically used in inexpensive handheld GNSS receivers. Adequate compensation for this frequency instability permits the long coherent integration intervals required to acquire and track GNSS signals with low carrier-to-noise ratios. The goal of this work is to push the use of GNSS deeper indoors or into environments where GNSS may be subject to interference.

I. INTRODUCTION

Despite strong incentives to push GNSS use further indoors, signal tracking in the weak-signal indoor environment remains a significant challenge. For indoor GNSS navigation, a receiver must track GNSS signals—which are already weak even under the best circumstances—after they experience severe (30–50 dB) attenuation caused by structural absorption [1].

Suppose a carrier-to-noise ratio, C/N_0, of 7 dB-Hz is chosen as a target for indoor GNSS signal acquisition. Then for a reasonably-sized search space and good detection statistics, a coherent integration duration of approximately 5 seconds is required. This translates into a requirement that the receiver's local reference oscillator maintain phase errors to a fraction of a cycle over those 5 seconds. This is impossible for current handheld GNSS receivers whose clocks are typically temperature-compensated crystal oscillators (TCXOs) with a frequency stability of 10^{-9} seconds at one second. At this stability level, TCXOs can only support coherent integration times of approximately 400 milliseconds. If the GNSS receiver clock were instead an oven-controlled crystal oscillator (OCXO) with a frequency stability at one second of 10^{-12} seconds, then a coherent integration duration of 10 seconds becomes possible.

Unfortunately, incorporating an OCXO-quality oscillator into an inexpensive, low-power, handheld GNSS receiver is currently impractical. Typical OCXOs are bench units that demand power and space. Small OCXOs designed for chip integration are expensive and are likely too large for most portable GNSS applications. Alternatives to OCXOs include high-stability embeddable oscillators such as chip-scale atomic clocks (CSACs). Current CSAC stability is on the order of 10^{-11} seconds at one second, but these models are under development and not yet available for sale. It is unlikely that manufacturers would immediately adopt CSACs given the cost and power requirements of CSACs versus TCXOs, although future development of CSACs may eventually make them feasible as stable oscillators in GNSS receivers [2–4].

Instead of replacing a GNSS receiver's inexpensive reference oscillator with an OCXO or CSAC, one can configure

Preprint of the 2010 ION GNSS Conference
Portland, OR, September 22–25, 2010

the receiver to create a "synthetic oscillator" by correcting phase errors during coherent integration based on a comparison with a non-GNSS signal of opportunity whose carrier frequency has OCXO-level stability. In other words, the receiver TCXO "leans" on this signal of opportunity for increased frequency stability. This technique is referred to as frequency stability transfer and is related to time and phase transfer [5–7].

Many commercial applications demand a highly stable time base. As a result, there are many candidate signals of opportunity that may prove useful for GNSS frequency stability transfer, including CDMA and GSM cell phone signals, NIST radio station signals, Iridium satellite pilot channels, and HDTV signals. During a period of GNSS availability, a GNSS receiver can make on-the-fly statistical characterizations to identify local signals with good stability [8]. Alternatively, the receiver may draw from a database of known stable signals. Later, when attempting to acquire or track GNSS signals in low C/N_0 environments, the receiver can use these pre-identified signals to phase correct the intermediate complex baseband outputs of the coherent summation interval using estimated phase errors calculated in a separate phase tracking loop that tracks the stable signal of opportunity.

The proposed strategy to extend the coherent integration time of a GNSS receiver clock will rely on these stable signals of opportunity. It will be shown that these external signals are stable enough to support GNSS signal acquisition and tracking in weak-signal environments.

II. REQUIRED COHERENT INTEGRATION TIME

Suppose that the indoor GNSS signal has attenuated to a $C/N_0 = 7$ dB-Hz and that the GNSS receiver is trying to coherently integrate to recover enough signal power to acquire and track. A natural question to ask is the following: how long does the receiver need to coherently integrate to acquire or track the GNSS signal? A theoretical lower bound that relates C/N_0 to the coherent integration time T will answer this question. Since weak-signal GNSS tracking first requires weak-signal GNSS acquisition, this lower bound will reflect the requirements of acquisition, which are stricter than those for tracking.

GNSS acquisition is essentially an exercise in hypothesis testing. A general GNSS acquisition statistic Z can be modeled as [9]

$$Z = \frac{1}{M} \sum_{l=1}^{K} \left| \sum_{k=1}^{M} \tilde{S}_k \right|_l^2 \tag{1}$$

where M is the number of coherent summations of complex baseband subaccumulations $\tilde{S}_k$ and K is the number of non-coherent summations. The relation between M and the coherent integration (or accumulation) time T is simply $T = MT_s$, where T_s is the subaccumulation period.

During acquisition, the receiver compares Z to a detection threshold chosen to satisfy a predetermined probability of false alarm P_{F}. Under the Neyman-Pearson lemma, the optimal detection threshold is based on the likelihood ratio $p(Z|H_1)/p(Z|H_0)$, where $p(Z|H_1)$ and $p(Z|H_0)$ are respectively the distributions of Z under the alternative hypothesis ("signal present") and the null hypothesis ("no signal present"). For GNSS acquisition, $p(Z|H_0)$ is Chi-squared with $2K$ degrees of freedom and $p(Z|H_1)$ is non-central Chi-squared with $2K$ degrees of freedom and non-centrality parameter $\lambda = KM\rho^2$. The signal-to-noise ratio (SNR) of the coherent accumulations, known as the pre-detection SNR or $\mathrm{SNR_{PD}}$, is related to ρ, T, and C/N_0 by

$$\mathrm{SNR_{PD}} = \rho^2/2 = T \cdot C/N_0. \tag{2}$$

For a given P_{F}, the probability of detection P_{D} can be increased by increasing M (longer coherent accumulations) or K (more non-coherent summations). Increasing M is most efficient in terms of minimizing the number of data samples required; therefore, the emphasis in this work is on extending coherent accumulation time.

In this paper, it is assumed that the bi-phase navigation bits that modulate data-bearing GNSS signals are known at the receiver, having been provided via some side channel. It is further assumed that the time offset due to initial position and time uncertainties amounts to a small fraction of a data bit interval. These provisions allow data bit transitions to be neglected in the analysis of coherent integration.

To acquire a GNSS signal, the receiver searches over a range of Doppler and code offsets, each corresponding to one of N search bins. Fixing $K = 1$ and setting $P_{\mathrm{F}} = 0.001$, one can calculate the value of $\mathrm{SNR_{PD}}$ required to achieve a minimum $P_{\mathrm{D}} = 0.95$ over a range of N. (These values for P_{F} and P_{D} lead to reliable acquisition and are typical of those used in practice.) The relation between $\mathrm{SNR_{PD}}$ and N is represented graphically in Fig. 1, which shows that an acquisition involving more search cells requires higher $\mathrm{SNR_{PD}}$.

By an iterative process, one can obtain an approximate target value of $\mathrm{SNR_{PD}}$ for indoor GNSS acquisition. Suppose $N = 500$ is taken as a rough initial guess of the number of search cells involved in acquisition. Then, according to Fig. 1, an approximate $\mathrm{SNR_{PD}}$ of 13.5 dB is required, which, given the assumed $C/N_0 = 7$ dB-Hz, implies a coherent integration time of $T = 13.5 - 7 = 6.5$ dB-seconds, or $T = 4.47$ seconds. This coherent integration time, in turn, implies a Doppler search granularity of approximately $\Delta f = 1/T = 0.22$ Hz. For civil GPS applications,

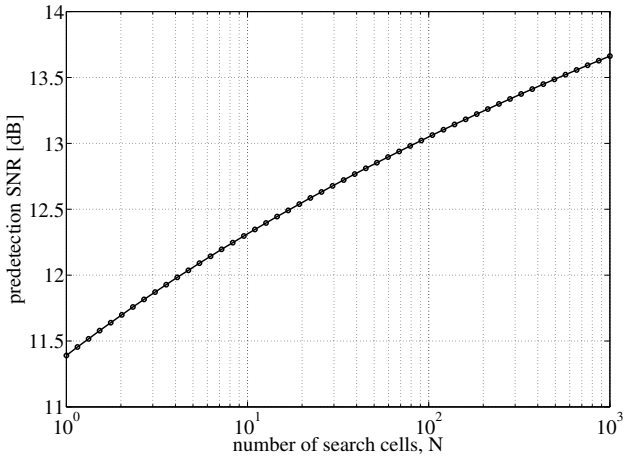

Fig. 1. Required pre-detection SNR to achieve $P_{\mathrm{D}} = 0.95$ as a function of the number of search bins N given a fixed $P_{\mathrm{F}} = 0.001$.

a reasonable code offset granularity can be set at 1/4 of a GPS L1 C/A code chip, or $\Delta t = 250$ nanoseconds. Then, supposing initial Doppler and position/timing uncertainty are respectively 1.6 Hz and 3.3 microseconds (these values will be justified later on in Section VI-C), a more accurate value for the number of required search cells N is obtained as $N = n_f n_t$, where $n_f = 1.6$ Hz$/\Delta f \approx 7.3$ and $n_t \approx 3.3$ μs$/\Delta t = 13.2$, leading to $N \approx 100$. This process can then be repeated with $N = 100$ as an initial guess for the number of search cells involved. For convenience in this paper, let an $\mathrm{SNR_{PD}}$ threshold equal to 13 dB (corresponding to $N = 100$ and $T \approx 4$ seconds at $C/N_0 = 7$ dB-Hz) be chosen as a rule-of-thumb threshold for reliable indoor acquisition.

One can think of tracking as repeated acquisition with a single search cell ($N = 1$). Therefore, from Fig. 1, the $\mathrm{SNR_{PD}}$ required to track given $P_{\mathrm{F}} = 0.001$ and $P_{\mathrm{D}} = 0.95$ is 11.4 dB. At the assumed indoor carrier-to-noise ratio $C/N_0 = 7$ dB-Hz, this implies a coherent integration interval of $T = 2.75$ seconds is sufficient for reliable indoor GNSS tracking.

These rule-of-thumb values for T presume that the receiver's local oscillator is perfectly stable over the coherent integration time required to meet the $\mathrm{SNR_{PD}}$ thresholds. The next section provides a model for oscillator behavior that will be useful for understanding how oscillator instability affects—and ultimately limits—the coherent integration time.

III. OSCILLATOR STABILITY

Characterization of oscillator stability is a mature field of study [10,11]. An oscillator with a sinusoidal, time-varying voltage $V(t)$ can be modeled as

$$V(t) = (V_0 + \epsilon(t)) \cos(2\pi\nu_0 t + \phi'(t)) \tag{3}$$

where V_0 is the nominal voltage amplitude, $\epsilon(t)$ is amplitude noise (usually neglected), ν_0 is the nominal center frequency, and $\phi'(t)$ is a time-varying phase (the $'$ on $\phi'(t)$ is meant to distinguish oscillator phase from GNSS carrier phase, which will be introduced in Sec. IV). The quantity of interest for the scope this paper is $\phi'(t)$, which, for a perfect oscillator, would remain constant for all time. The instantaneous frequency $\nu(t)$ is defined as the time derivative of the total phase normalized by 2π radians:

$$\nu(t) = \nu_0 + \frac{1}{2\pi}\frac{d}{dt}\phi'(t). \tag{4}$$

Additionally, the fractional frequency deviation $y(t)$, useful for comparing oscillators running at different center frequencies, is defined as the time derivative of phase normalized by $2\pi\nu_0$:

$$y(t) \equiv \frac{1}{2\pi\nu_0}\frac{d}{dt}\phi'(t). \tag{5}$$

For a constant $\phi'(t)$, it follows that $\nu(t) = \nu_0$ and $y(t) = 0$; however, variations in $\phi'(t)$ lead to variations in $\nu(t)$ and to $y(t) \neq 0$.

Many applications require a quantitative measure of the stability of an oscillator over a specific time duration τ. For this, it is convenient to introduce the average fractional frequency deviation, defined as

$$\bar{y}_k = \frac{1}{\tau}\int_{t_k}^{t_k+\tau} y(t)dt. \tag{6}$$

A natural metric for stability over an interval would be the standard statistical variance of $\bar{y}_k$; however, the standard variance fails to converge for certain phase noise processes. Instead, the two-sample or Allan variance $\sigma_y^2(\tau)$ defined by

$$\sigma_y^2(\tau) = \left\langle \frac{(\bar{y}_{k+1} - \bar{y}_k)^2}{2} \right\rangle \tag{7}$$

with $\tau = t_{k+1} - t_k$ (no dead time between measurements) is commonly used to measure the stability of oscillators [12]. By way of illustration, at $\tau = 1$ second, the Allan deviation $\sigma_y(\tau)$ for a typical TCXO is about 10^{-9} whereas a typical OCXO is roughly 1000 times more stable, or $\sigma_y(\tau = 1 \text{ sec}) = 10^{-12}$.

Another useful metric for comparing oscillators is the coherence function C_{coh}:

$$C_{\mathrm{coh}}(T) = \left| \frac{1}{T}\int_0^T e^{j\phi'(t)}dt \right|, \qquad 0 \leq C_{\mathrm{coh}}(T) \leq 1. \tag{8}$$

The coherence function expresses the effects of variations in $\phi'(t)$ during coherent integration as a decline from unity as T increases.

With an oscillator model and metrics characterizing oscillator stability established, the next section introduces a model for GNSS carrier phase that reveals the connection between oscillator variations and measured carrier phase variations.

IV. THE EFFECT OF OSCILLATOR INSTABILITY ON MEASURED CARRIER PHASE

Consider the following model for the GNSS beat carrier phase, $\phi(t)$, commonly referred to as the carrier phase observable [13]:

$$\lambda\phi(t) = r(t) + c[\delta t_R(t) - \delta t_S(t)] + \lambda(\gamma_0 - \psi_0) + \epsilon_{\text{atmo}}(t) + \lambda n_\phi. \quad (9)$$

Here, $r(t)$ is the range from the receiver to the satellite, c is the speed of light, $\delta t_R(t)$ is the instantaneous receiver clock offset from true GPS time, $\delta t_S(t)$ is the instantaneous satellite clock offset from true GPS time, λ is the wavelength of the GNSS signal, $(\gamma_0 - \psi_0)$ represents a constant phase offset between the GNSS receiver and satellite carrier phases, $\epsilon_{\text{atmo}}(t)$ represents the variations due to atmospheric effects (ionospheric and tropospheric), and n_ϕ is measurement noise due to wideband thermal noise in the receiver front end. The quantity $\delta t_R(t)$ is related to the receiver clock's phase departure $\phi'(t)$ by

$$\phi'(t) = 2\pi \cdot \delta t_R(t) \cdot \nu_0. \quad (10)$$

To illustrate the effects of the different components in this model, consider an experiment whereby the carrier phase observable is measured with a GPS receiver driven by a TCXO and later by an OCXO, with each recording lasting 10 minutes. After the carrier phase measurements are recorded, the data are post-processed to remove the deterministic carrier phase variations due to the effects of the satellite orbit. Low-frequency components remaining in the data are presumed to be due to ionospheric errors, ephemeris errors, errors in the timing of the range calculations, or errors in the approximate receiver position. The latter three errors are substantially eliminated by a linear fit to the carrier phase time history, an operation which does not alter the stability of the phase time history and which can be implemented by Fourier-transform techniques in real-time processing. What remains in the phase time history after such processing are the unpredictable components of Eq. 9, which will be referred to as the *non-deterministic* components hereafter.

Figures 2 and 3 show the results of such an experiment. Here, the estimated non-deterministic carrier phase components for four GPS signals identified by their pseudo-random-number (PRN) code are displayed, with Fig. 2 showing the TCXO-driven case and Fig. 3 showing the OCXO-driven case. What is immediately clear from the two figures is the superior stability of the OCXO relative to the TCXO: whereas the TCXO phase ranges from -1200 to 750 radians over a 10 minute interval, the OCXO remains within ±6 radians.

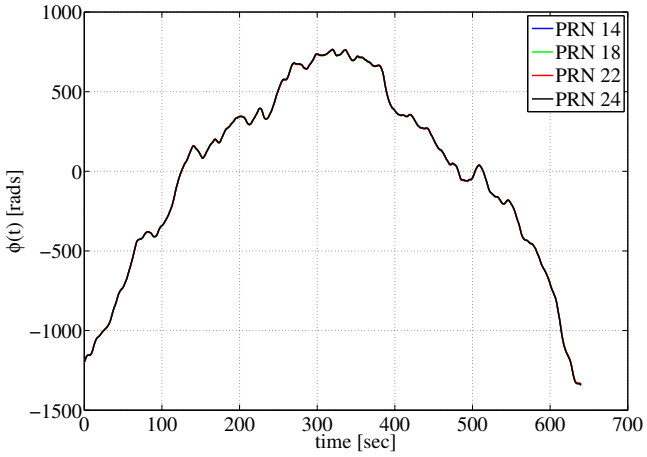

Fig. 2. Estimated non-deterministic TCXO-driven carrier phase over a ten minute recording. Note that four channels are actually plotted in this figure but the small ±4 radian differences are imperceptible on this scale.

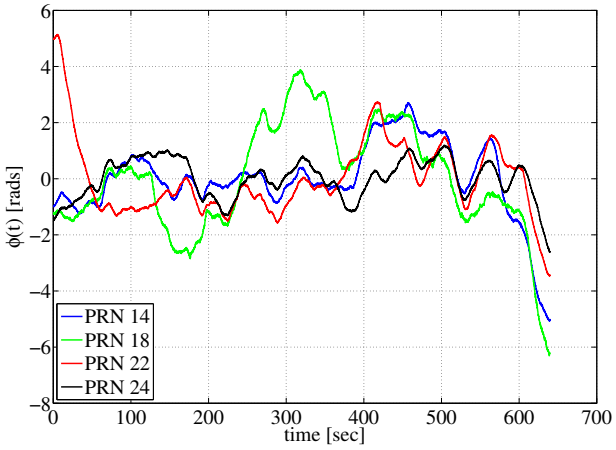

Fig. 3. Estimated non-deterministic OCXO-driven carrier phase over a ten minute recording.

For more insight into these two plots, first consider Eq. 9 with respect to the TCXO phase estimate shown in Fig. 2. The effect of range $r(t)$ was eliminated in the data post-processing. Similarly, the effect of the instantaneous satellite clock offset $\delta t_S(t)$ was substantially eliminated by applying the broadcast linear correction. The offset $(\gamma_0 - \psi_0)$ remains constant so long as neither receiver nor satellite is power cycled during the recording and is therefore eliminated as part of the detrending operation. The phase noise component n_ϕ amounts to high-frequency noise, only adding "fuzz" to the plots. This leaves as non-deterministic components the unpredictable effects of at-

mosphere, $\epsilon_{\text{atmo}}(t)$, and the instantaneous receiver clock offset, $\delta t_R(t)$. This latter quantity is by far the most significant component in what remains of the TCXO-driven carrier phase observable. Hence, this experiment amounts to a comparison of two oscillators, with the TCXO playing the role of the oscillator under test and each atomic clock aboard the GPS satellites playing the role of the reference oscillator. As the TCXO is much less stable than the atomic oscillators, the phase variations in Fig. 2 reflect the stability of the TCXO.

Now consider Eq. 9 with respect to the OCXO phase estimates shown in Fig. 3. Again, $r(t)$ and $(\gamma_0 - \psi_0)$ have been eliminated and n_ϕ contributes only "fuzz" to the variations. But now the driving oscillator is an OCXO, so the effects of $\delta t_R(t)$ have been reduced significantly, allowing the effects of $\epsilon_{\text{atmo}}(t)$ and potentially even $\delta t_S(t)$ to show. Common-mode variations in the phase-time history reflect instability in the local OCXO, but non-common-mode variations must be due to $\delta t_S(t)$ or $\epsilon_{\text{atmo}}(t)$, which are both unique to each PRN.

The non-deterministic components of the measured carrier phase shown in Figs. 2 and 3 can be treated as the instantaneous carrier phase departure $\phi'(t)$ in the oscillator model of Eq. 3 for purposes of assessing the limits of coherent integration within a GNSS receiver. This implies that coherent integration is limited by local clock variations $\delta t_R(t)$, by errors due to atmospheric variations $\epsilon_{\text{atmo}}(t)$, and, to a lesser extent, by satellite clock variations $\delta t_S(t)$.

Treating the lumped non-deterministic components of the measured carrier phase as the phase departure $\phi'(t)$ in Eq. 3 permits application of the metrics developed in Sec. III to characterize the stability of the unpredictable GNSS carrier phase components—the components that limit coherent integration time. An Allan deviation plot is presented in Fig. 4 for the GPS satellite with highest C/N_0 over the recording intervals, PRN 22. That the OCXO's $\sigma_y(\tau)$ values are smaller than the TCXO's come as no surprise given the OCXO's greater stability.

A rough approximation for the coherence time T_{coh}, or the maximum time over which the oscillator can support coherent integration, is obtained directly from the Allan deviation as the value of τ satisfying [14]

$$2\pi\nu_0 \cdot \sigma_y(\tau) \cdot \tau \;\approx\; 1 \text{ radian.} \tag{11}$$

More precisely, T_{coh} is defined as the value of T for which the mean-squared coherence function $\langle C^2_{\text{coh}}(T)\rangle$ drops below 0.5. The mean-squared coherence function computed for the non-deterministic TCXO- and OCXO-driven carrier phase estimates is shown in Fig. 5 for PRN 22. For the TCXO, $T_{\text{coh}} < 0.4$ seconds whereas for the OCXO, $T_{\text{coh}} > 100$ seconds.

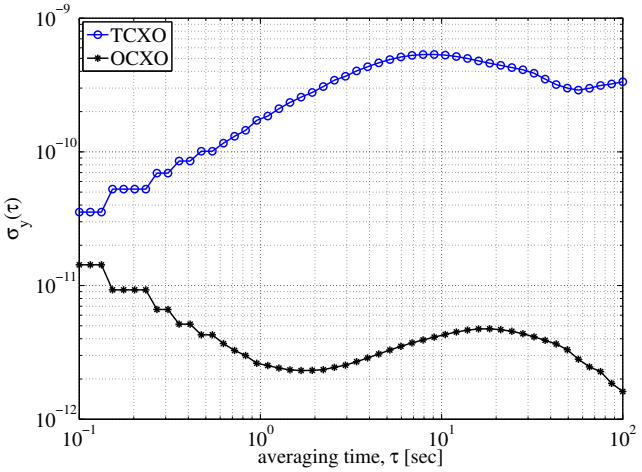

Fig. 4. Allan deviation for the non-deterministic TCXO- and OCXO-driven carrier phase estimates corresponding to PRN 22.

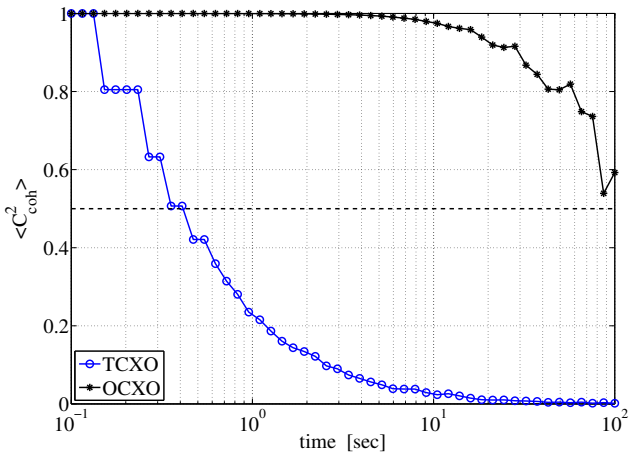

Fig. 5. Mean-squared coherence of the non-deterministic TCXO- and OCXO-driven carrier phase estimates of PRN 22.

The mean-squared coherence function $\langle C^2_{\text{coh}}(T)\rangle$ can be incorporated into the SNR_{PD} model from Eq. 2 to account for the instability of the driving oscillator:

$$\text{SNR}_{\text{PD}}(T) = \langle C^2_{\text{coh}}(T)\rangle \cdot T \cdot C/N_0. \tag{12}$$

Figure 6 plots Eq. 12 with the experimentally-derived mean-squared coherence functions for the TCXO and the OCXO. Clearly, the TCXO is not stable enough to reach the SNR_{PD} acquisition or tracking thresholds regardless of the duration of coherent integration time, whereas the OXCO meets the acquisition threshold after 4 seconds. The goal of the next section is to present a method for extending a TCXO's coherence time to that of an OCXO.

V. FREQUENCY STABILITY TRANSFER

Frequency stability transfer is a method for transferring the frequency stability of a remote oscillator to a local

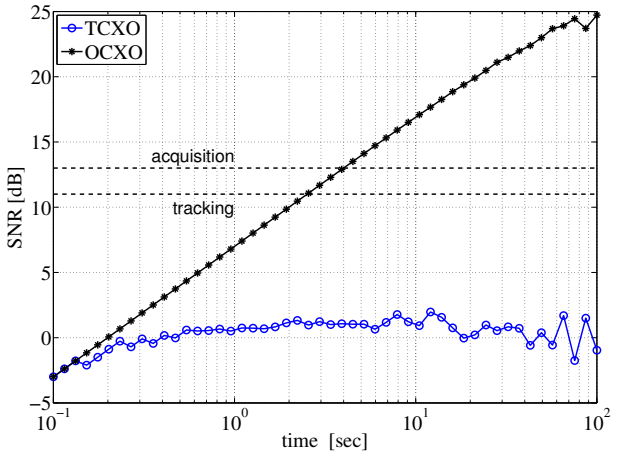

Fig. 6. Pre-detection SNR for TCXO- and OCXO-generated carrier phase estimates for an assumed $C/N_0 = 7$ dB-Hz.

application. In the context of weak-GNSS-signal tracking, frequency stability transfer is the exercise of compensating for the local oscillator's phase instability by applying phase corrections derived from a stable aiding signal. Because many commercial applications require highly stable oscillators to drive their radio frequency transmissions, there are many potential ambient radio signals that could supply a GNSS receiver with phase corrections; such signals are called signals of opportunity. A simple frequency stability transfer model illustrates how the method can be implemented in a GNSS receiver and establishes selection criteria for signals of opportunity.

A. Simple Frequency Stability Transfer Model

A model for frequency stability transfer fits naturally into a general GNSS receiver framework as shown in Fig. 7. In the GNSS signal processing chain, the receiver despreads and mixes to baseband the received GNSS signal $\mathbf{r}_{\text{GNSS}}$ by multiplying it with a local signal replica, $C_{\text{GNSS}}e^{j\theta}$. The product is summed to yield a complex intermediate accumulation S. The phase corresponding to each S in a given sequence of $S_1, S_2, \ldots, S_{N_S}$ varies slightly from one intermediate accumulation to the next due to local-oscillator-induced phase variations. If the local oscillator has poor stability and the sequence $S_1, S_2, \ldots, S_{N_S}$ is summed without correcting for these phase variations, then the intermediate accumulations decohere, eventually interfering with each other destructively and diminishing the magnitude of the final accumulation $S = S_1 + S_2 + \ldots + S_{N_S}$. In other words, with a low-cost local oscillator that has poor stability, the SNR_{PD} of the final accumulations would never reach thresholds required for acquisition or tracking.

To extend the coherent summation duration, the rotation block in Fig. 7 applies a phase correction to each intermediate accumulation S: each S is rotated by an estimate $\Delta\phi$ of the local-oscillator-induced phase change over the

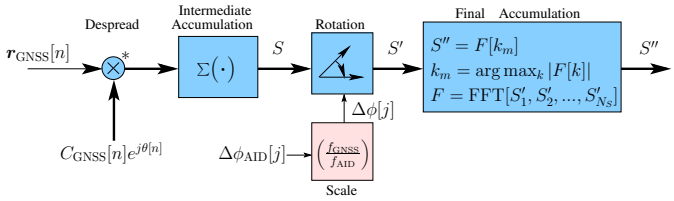

Fig. 7. Block diagram model for frequency stability transfer in a general GNSS receiver. Thick arrows denote complex signal routing; the asterisk $*$ denotes complex multiplication.

intermediate accumulation interval. The phase correction term applied to S_j at the jth intermediate accumulation interval is

$$\Delta\phi[j] = \left(\frac{f_{\text{GNSS}}}{f_{\text{AID}}}\right) \cdot \left(\phi_{\text{AID}}[n_j] - \phi_{\text{AID}}[n_{j-1}]\right). \qquad (13)$$

Here, $\phi_{\text{AID}}[n_j] - \phi_{\text{AID}}[n_{j-1}]$ is the difference in the aiding signal's phase at the boundaries of the jth intermediate accumulation interval. The aiding signal's phase ϕ_{AID} can also be modeled by Eq. 9 although the effect of atmospherics ϵ_{atmo} is negligible. If the aiding signal is generated by a stable frequency source, and if its local phase measurement is referenced to the same local oscillator that drives the phase of S, then the aiding signal's phase shifts, after scaling by the ratio of the GNSS and aiding frequencies $f_{\text{GNSS}}/f_{\text{AID}}$, are an estimate of the local oscillator's phase shifts over the intermediate accumulation intervals.

The measurement of the aiding signal's phase change includes phase noise n_ϕ due to front-end thermal noise. Depending on the aiding signal's center frequency, this noise is either attenuated or magnified by the scaling $f_{\text{GNSS}}/f_{\text{AID}}$. All else being equal, higher frequency aiding signals are preferred.

Applying $\Delta\phi$ to S to correct for the local-oscillator-induced phase variations generates the phase-corrected S'. To form the final accumulation S'', the receiver computes the fast Fourier transform (FFT) of a set of phase-corrected intermediate accumulation values; that is $F = \text{FFT}[S'_1, S'_2, \ldots, S'_{N_S}]$. The discrete frequency k_m that maximizes $|F(k_m)|$ is selected, and the final accumulation $S'' = F[k_m]$.

The FFT-based final accumulation operation removes any constant frequency offsets present in the sequence $S'_2, \ldots, S'_{N_S}$ due to a possible offset between the aiding signal's advertised and actual transmitted center frequency. This means that the proposed frequency stability transfer strategy can tolerate small frequency offsets, so long as these remain constant; hence, the technique is referred to as "frequency stability transfer" as opposed to "frequency transfer."

With the model for frequency stability transfer developed,

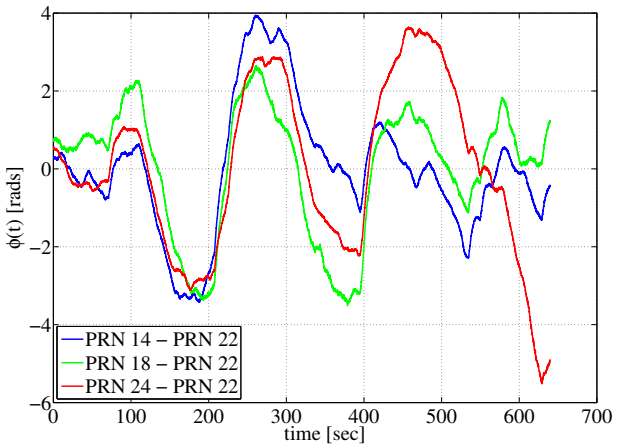

Fig. 8. The resulting SYXO carrier phase estimate after differencing the non-deterministic TCXO-driven carrier phase measurements.

a simple experiment demonstrates the potential and limitations of the technique.

B. Synthetic Oscillator Experiment

Suppose the non-deterministic TCXO-driven carrier phase estimate for PRN 22 from Sec. IV is chosen as the aiding signal and is subtracted from the remaining three PRN phase estimates. In the frequency stability framework, $\Delta\phi = \Delta\phi_{\text{PRN22}}$ with $f_{\text{GNSS}}/f_{\text{AID}} = 1$. This procedure is equivalent to performing a single-difference carrier phase measurement to eliminate phase variations due to the receiver's local oscillator [13].

Figure 8 shows the resulting phase time history, which one can think of as being associated with a virtual local oscillator at the receiver, the "synthetic oscillator" (SYXO), whose stability is as good as the inherent stability of the aiding signal, in this case derived from PRN 22. The "SYXO-referenced" carrier phase estimate varies approximately ± 4 radians over the 10 minute window. The variations observed in the SYXO phase history are comparable to the ± 6 radian variations in the non-deterministic OCXO-driven carrier phase, which suggests that the SYXO carrier phase history is roughly as stable as the OCXO-driven carrier phase. Setting $\tau = 10$ seconds and applying Eq. 11 to the SYXO phase history yields a value of 0.38 radians, indicating that the SYXO remains coherent at 10 seconds and would allow the receiver to produce the SNR_{PD} required for weak-signal acquisition and tracking.

When applied in the context of the foregoing model for frequency stability transfer, exploiting a strong GNSS signal as the aiding signal is similar to the technique advanced in Ref. [15] for estimating a GNSS receiver's local clock variations. Obviously, in weak-GNSS-signal environments it may be the case that all GNSS signals are severely attenuated, leaving none available for use as an aiding signal. This motivates the search for stable ambient aiding signals that can be tracked indoors.

VI. SIGNALS OF OPPORTUNITY

Although there are several ambient stable frequency sources, not all are suitable for frequency stability transfer. This section considers three candidate signals of opportunity.

A. NIST WWVB and WWV Timing Signals

The National Institute of Standards and Technology (NIST) operates an ensemble of atomic oscillators whose timing is broadcast throughout the world [16]. NIST continually broadcasts a 60 kHz low-frequency-band radio signal, WWVB, and a 5, 10, and 15 MHz signal, WWV, from Fort Collins, Colorado. These signals are designed to aid radio-controlled clock calibration—calibration of the so-called "atomic" clocks that set their own time to the WWVB or WWV reference.

Unfortunately, these NIST signals are not good candidates for frequency stability transfer in the current context of weak-GNSS-signal tracking because their frequencies are low compared to those of GNSS. With WWVB or WWV as an aiding signal, the large scaling ratio $f_{\text{GNSS}}/f_{\text{AID}}$ ($\sim$26,000 for WWVB and $\sim$157 for WWV) would tend to greatly magnify the phase noise on the aiding measurements, preventing the inherent stability of the signals from being harnessed at GNSS frequencies.

B. High-Definition Television (HDTV)

High-definition television (HDTV) holds potential for frequency stability transfer because the signals are exceptionally strong (they were designed to penetrate into buildings where most TV tuners reside) and are available in all major metropolitan areas in the U.S. [1]. The broadcast frequency, at around 700 MHz, is lower than GNSS center frequencies, which tends to amplify the phase noise in the frequency transfer model, though the effect is much more benign than with the NIST signals (a factor of $\sim$2 versus factors of $\sim$26,000 or $\sim$157). HDTV may be pursued as an aiding signal in future work, but for the initial proof-of-concept, a higher-frequency aiding signal was sought.

C. Cellular CDMA Signals

Code division multiple access (CDMA) cellular signals are excellent frequency-stability-transfer candidates for several reasons: (1) they are available in both urban and rural environments; (2) they penetrate buildings; (3) they are broadcast with a structure similar to GNSS; (4) they are transmitted in the 1900 MHz band; and (5) they have dataless pilot channel that is referenced to a highly-stable clock.

Modern CDMA basestations and cellular handsets follow

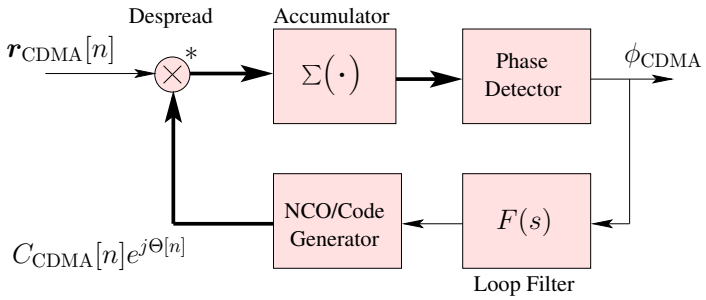

Fig. 9. A block diagram for CDMA acquisition of the pilot channel that includes a phase tracking loop to extract estimates of the CDMA carrier phase.

the CDMA 2000 standard while providing backwards compatibility with the older IS-95 standard. Under these standards, basestations are required to maintain time accuracy to within 10 microseconds of GPS time [17]. Such synchronization allows basestations to distinguish themselves and prevent interference by broadcasting the same pseudorandom noise (PN) sequence at unique time offsets. Many cellular companies use highly-stable, GPS-synchronized oscillators in their CDMA basestations to continue to meet this requirement for up to 36 hours in the event of a GPS outage.

For opportunistic frequency stability transfer, the GNSS receiver only needs to make use of the downlink (the link from basestation to mobile) as opposed to the uplink (the link from the mobile to the basestation). The basestations continually transmit a dataless pilot channel to synchronize with mobile devices. This pilot channel is derived directly from the basestation's stable timebase, providing a receiver with a reliable, steady, and accurate frequency reference that can be acquired and tracked without the need for bit synchronization.

The pilot channel consists of a repeating 32,768-chip PN sequence transmitted at a rate of 1.2288 mega-chips per second. To synchronize with the pilot channel, a receiver can correlate the received signal against its own local replica and then employ standard code and phase tracking loops to estimate the carrier phase of the CDMA signal, as shown in the block diagram of Fig. 9.

A preliminary study supporting this paper suggests that the actual carrier frequencies of the CDMA downlink are accurate to within 1.6 Hz of the advertised values, and that synchronization with the PN sequence and subsequent decoding of the so-called synchronization channel permits synchronization with GPS time to within less than 1 μs. Adding 2.3 μs to this timing uncertainty to account for initial position uncertainty yields the 1.6 Hz and 3.3 μs Doppler and timing uncertainty intervals introduced in the rule-of-thumb calculations of Section II.

The frequency of CDMA downlink cellular signals is in the 1900 MHz band. Each basestation transmits at a center frequency between 1931.25 and 1988.75 with a bandwidth of 1.25 MHz. Since these broadcast center frequencies are higher than GNSS frequencies, the measurement noise on the CDMA phase estimates is attenuated in Eq. 13, allowing the full inherent stability of the CDMA signals to be passed on to a GNSS receiver in the frequency stability transfer framework.

VII. FREQUENCY STABILITY TRANSFER VIA SIGNALS OF OPPORTUNITY

The general model of frequency stability transfer involves parallel acquisition and tracking paths for the a GNSS signal and for a stable aiding signal. The complete frequency stability transfer model is shown in Fig. 10 in block diagram form. Here, the aiding signal's phase corrections to the local-oscillator-induced phase variations are output from a general code and carrier phase tracking loop.

The software-defined GRID GNSS receiver [18–20] was augmented to acquire and track cellular CDMA signals in addition to GNSS signals. The receiver measured and recorded the carrier phase estimates from GPS L1 C/A and cellular CDMA signals, with both the GPS and cellular CDMA tracking loops tied to the same local oscillator. CDMA phase data corresponding to different basestations transmitting at 1935 MHz and 1952.5 MHz were recorded. As explained in Sec. IV, a linear fit removed the deterministic components of the GPS carrier phase observable. A linear fit was also applied to the CDMA carrier phase to remove any linear trends. The detrended CDMA carrier phase estimate was then scaled by the ratio given in Eq. 13 and subtracted from the non-deterministic GPS carrier phase estimate. This process generated a CDMA-aided carrier phase history that eliminated the phase variations of the receiver's local oscillator. This experiment assumed

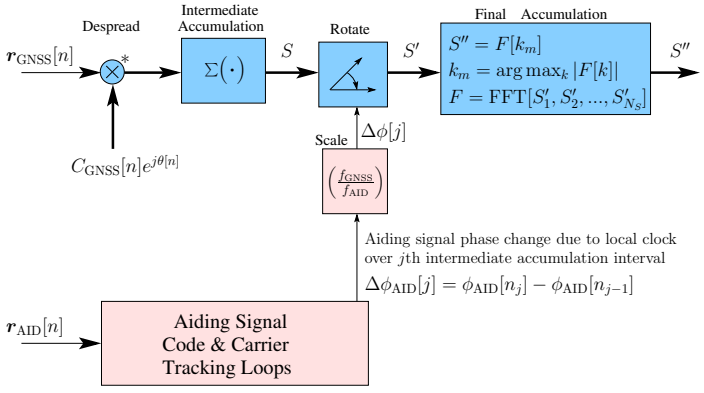

Fig. 10. A block diagram illustrating frequency stability transfer that makes use of two parallel acquisition and tracking paths, one for a GNSS signal and one for an aiding signal. The aiding signal's phase corrections compensate for the local-oscillator-induced phase variations over each intermediate accumulation interval.

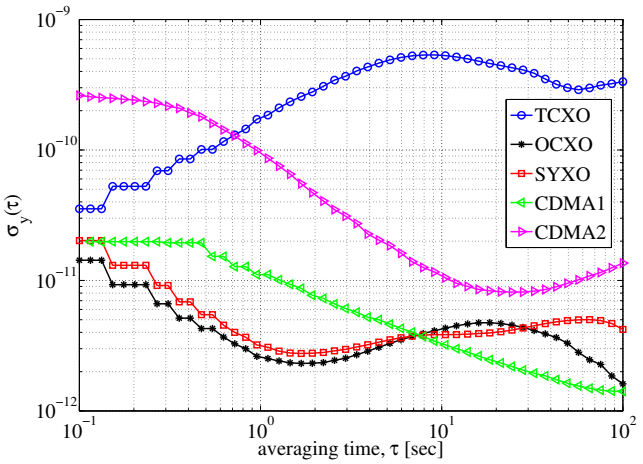

Fig. 11. Allan deviation for the non-deterministic TCXO- and OCXO-driven carrier phase estimates, non-deterministic SYXO carrier phase, and the two CDMA-aided carrier phase estimates.

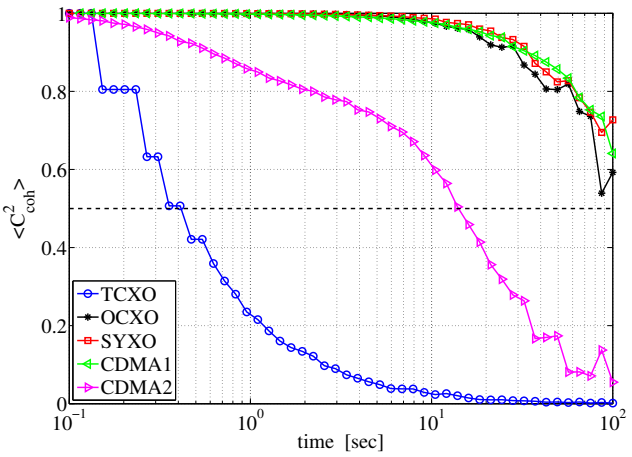

Fig. 12. Mean-squared coherence for the non-deterministic TCXO- and OCXO-driven carrier phase estimates, non-deterministic SYXO carrier phase, and the two CDMA-aided carrier phase estimates.

the receiver knew its approximate position and time and remained stationary over the experiment interval.

The CDMA-aided carrier phase estimate can be evaluated with the metrics in Sec. III to characterize its stability. A plot of the Allan deviation generated from two CDMA-aided carrier phase estimates (CDMA1 and CDMA2) is shown in Fig. 11. The same TCXO and OCXO results from Sec. IV are included for reference as well as the results from the SYXO of Sec. V-B. The stability of the two CDMA-aided phase estimates is between 10^{-11} and 10^{-12} at $\tau = 10$ seconds. Note that the stability of CDMA1 and CDMA2 is roughly bounded by the TCXO and OCXO between 1 and 10 seconds. Applying the approximate coherence time calculation from Eq. 11 and setting $\tau = 10$ seconds, CDMA1 yields a value of 0.32 radians and CDMA2 yields a value of 0.98 radians. Thus, both are approximately coherent at 10 seconds.

The mean-squared coherence function $\langle C^2_{\text{coh}}(T)\rangle$ for the data sets can be compared as shown in Fig. 12 where the TCXO, OCXO, and SYXO results are also included. The CDMA-aided phase estimates have a coherence time ranging from 10 seconds to beyond 100 seconds. The difference in the two CDMA-aided phase data sets is intriguing and will be the subject of future research.

Because different aiding signals will have different inherent stability, receivers implementing frequency stability transfer would benefit from a database of local ambient stable signals or from on-the-fly statistical characterizations of signals of opportunity during periods of GNSS availability [8]. Once the receiver enters a weak-signal environment, it tracks the best aiding signal among those available and applies phase corrections to increase SNR_{PD} through coherent integration.

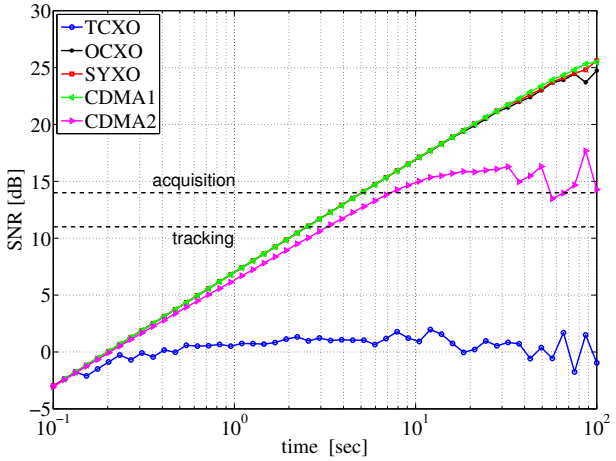

Fig. 13. SNR_{PD} as a function of coherent integration time for the non-deterministic TCXO- and OCXO-driven carrier phase estimates, non-deterministic SYXO carrier phase, and the two CDMA-aided carrier phase estimates, assuming $C/N_0 = 7$ dB-Hz.

The benefit of this frequency stability transfer technique is evident in Fig. 13, which plots Eq. 12 as a function of integration time for a GPS signal with nominal $C/N_0 = 7$ dB-Hz. Whereas the short coherence time of the low-cost TCXO prevents it from ever reaching the target thresholds for acquisition and tracking, the CDMA-cellular-signal-aided low-cost local oscillator can sustain long coherence times: CDMA1 reaches this goal at 5 seconds and CDMA2 reaches this goal at 8 seconds. This shows that CDMA is indeed a viable candidate signal of opportunity for frequency stability transfer.

VIII. CONCLUSION

A preliminary study of frequency stability transfer indicates that it is possible to acquire and track extremely weak (∼7 dB-Hz) GNSS signals using inexpensive local oscillators whose phase variations are compensated by phase measurements of ambient CDMA-cellular "signals of opportunity." The proposed strategy for extended coherent integration assumes either that a dataless GNSS signal (e.g., GPS L2CL) is being acquired or tracked or that the navigation data bit sequence is known to the receiver. It further assumes that the receiver travels at a predictable velocity or is substantially stationary during the interval of coherent integration (position variations that are a small fraction of the GNSS and aiding carrier wavelengths are allowed). Thus, the method in this paper would be well-suited for "snapshot" indoor positioning.

ACKNOWLEDGMENTS

This work was generously supported in part by the Department of Defense through the National Defense Science and Engineering Graduate Fellowship Program. Thanks also to the members of The University of Texas at Austin Radionavigation Laboratory and the Wireless Networking and Communications Group.

NOTE

The University of Texas at Austin is in process of applying for a patent to cover the frequency stability transfer technique described herein.

References

[1] Rabinowitz, M. and Spilker, Jr., J. J., "Augmenting GPS with Television Signals for Reliable Indoor Positioning," *NAVIGATION, Journal of the Institute of Navigation*, Vol. 41, No. 4, 2004, pp. 269–287.

[2] Lutwak, R., Emmonds, D., English, T., and Riely, W., "The Chip-Scale Atomic Clock—Recent Development Progress," *Proc. 34th Ann. Precise Time and Time Interval Systems Applications Meeting*, December 2003.

[3] Mescher, M., Lutwak, R., and Varghese, M., "An ultra-low-power physics package for a chip-scale atomic clock," *The 13th Intl. Conf. on Solid-State Sensors, Actuators and Microsystems*, Vol. 1, June 2005, pp. 311–316.

[4] Lutwak, R., "The Chip-Scale Atomic Clock—Recent developments," *IEEE Intl. Freq. Control Symp.*, April 2009, pp. 573–577.

[5] Larson, K. M. and Levine, J., "Carrier-Phase Time Transfer," *IEEE Transactions on Ultrasonics, Ferroelectrics, and Frequency Control*, Vol. 46, 1999, pp. 1001–1012.

[6] Levine, J., "A Review of Time and Frequency Transfer Methods," *Meterologia*, Vol. 45, 2008, pp. S162–S174.

[7] Schildknecht, T. and Springer, T., "High Precision Time and Frequency Transfer Using GPS Phase Measurements," *Proc. 30th Ann. Precise Time and Time Interval Meeting*, Reston, VA, 1998.

[8] Petovello, M. and Lachapelle, G., "Using Standalone GPS to Evaluate Precise Oscillator Stability in the Time Domain," *Proc. of ION GPS*, Nashville, TN, September 1999, pp. 1081–1089.

[9] Van Dierendonck, A. J., *Global Positioning System: Theory and Applications*, chap. 8: GPS Receivers, American Institute of Aeronautics and Astronautics, 1996, pp. 329–407.

[10] Sullivan, D., Allan, D., Howe, D., and Walls, F., "Characterization of Clocks and Oscillators," Tech. rep., National Institue of Standards and Technology, 1990.

[11] Rutman, J., "Characterization of Frequency Stability in Precision Frequency Sources," *Proc. IEEE*, Vol. 79, 1991, pp. 952–960.

[12] Allan, D. W. and Barnes, J. A., "A Modified "Allan Variance" with Increased Oscillator Characterization Ability," *Proc. 35th Ann. Freq. Control Symposium*, 1981.

[13] Psiaki, M. and Mohiuddin, S., "Modeling, analysis, and simulation of GPS carrier phase for spacecraft relative navigation," *Journal of Guidance Control and Dynamics*, Vol. 30, No. 6, 2007, pp. 1628.

[14] Thompson, A. R., Moran, J. M., and Swenson, Jr., G. W., *Interferometry and Synthesis in Radio Astronomy*, Wiley and Sons, 1986.

[15] Morrison, A., "Accurate Milisecond Level Oscillator Phase Noise Estimation for Standalone GNSS," *Proc. ION GNSS Conf.*, Savannah, GA, 2009.

[16] Lombardi, M. A., "NIST Time and Frequency Services," Tech. rep., National Institute of Standards and Technology, 2002.

[17] Almaimani, M., Korsuwana, P., Twine, M., and Mendelsohn, J., "IMT-2000: A Comparative Analysis of cdma2000 and UTRA," http://citeseerx.ist.psu.edu/viewdoc/summary?doi=10.1.1.29.5540.

[18] Humphreys, T. E., Ledvina, B. M., Psiaki, M. L., and Kintner, Jr., P. M., "GNSS Receiver Implementation on a DSP: Status, Challenges, and Prospects," *Proceedings of ION GNSS 2006*, Institute of Navigation, Fort Worth, TX, 2006.

[19] O'Hanlon, B. W., Psiaki, M. L., Kintner, Jr., P. M., and Humphreys, T. E., "Development and Field Testing of a DSP-Based Dual-Frequency Software GPS Receiver," *Proceedings of ION GNSS 2009*, Institute of Navigation, Savannah, GA, 2009.

[20] Humphreys, T., Bhatti, J., and Ledvina, B., "The GPS Assimilator: a Method for Upgrading Existing GPS User Equipment to Improve Accuracy, Robustness, and Resistance to Spoofing," *Proceedings of the ION GNSS Conference*, Institute of Navigation, Portland, Oregon, 2010.